GILDA Annual Report 2013

December 2013
Issue 1

Contents:

Foreword

The year 2013 has represented a turning point after the severe difficulties experienced in 2012.
The beamline personnel has raised to three units thanks to the creation of one post doctoral position. Regular calls for proposals on the CRG beamtime quota have been launched in May and November 2013. A new Proposal Review Panel for the Italian beamtime has come into operation and a new proposal submission procedure has been implemented, based entirely on the ESRF web site (see the guidelines for beamtime applications on the last page of this report).
This has permitted a gradual return to normal conditions for beam delivery to users.
In 2013, 411 shifts have been dedicated to user mode and 24 experiments have been carried out. The remaining 216 shifts were dedicated to different activities such as In House research, training of the new staff member, test of new protocols for beamline control and semi-automatic alignment and commissioning of new experimental apparata. No major instrumentation breakdown has occurred this year allowing the beamline staff and users to fully take advantage of the beamtime delivered by the ESRF source.
The scientific activity has been intense with the development a new technique for in-situ studies of electrochemical processes (also selected for the ESRF 2013 Highlights), the commissioning of a cryostat for the collection of XAS data on frozen solutions at liquid nitrogen temperature and the launch of programs like pump-probe experiments, large area x-ray fluorescence mapping, XEOL data collection (see the News from the beamline Section for more details).
Looking to the future, 2014 will be the year of the periodic evaluation by the ESRF Beamline Review Panel and for the definition of the beamline refurbishment program taking into account the opportunities offered by the new lattice of ESRF foreseen in the phase II of the Upgrade Program.

Francesco d'Acapito, scientist in charge

Istituto Officina dei Materiali

INFN Istituto Nazionale di Fisica Nucleare Laboratori Nazionali di Frascati

Written and edited by: Francesco d'Acapito, Angela Trapananti and Simona Torrengo (CNR-IOM-OGG Grenoble)

GILDA c/o ESRF, 6 rue Jules Horowitz , 38043 Grenoble Cedex 9, France
Tel: +33 (0)476882085 - http://www.esrf.eu/UsersAndScience/Experiments/CRG/BM08 - e-mail: dacapito@esrf.fr

A new apparatus for x-ray excited optical luminescence (XEOL) experiments

An apparatus for the collection of the optical emission from the sample following the x-ray excitation has been developed and successfully tested.
The aim was to make available an additional XAS data collection mode that is capable to provide information on the luminescent regions of the sample.
The apparatus consists in a collector bearing two lenses, one to collect light from the sample and the other for the focalization on an optical fiber. The system provides a moderate demagnification of a factor 1.6 in order to feed the entire image of the sample into the fiber. The lenses are made of BK7 glass and have a transparency range between 350 nm and 2000 nm. The collector is inserted in a vacuum chamber in order to allow measurements also at low temperature (liquid nitrogen). The optical signal is sent to the detector via an optical silica fiber passing through the vacuum environment. The fiber is 10 m long and it can be drawn even outside the experimental hutch if needed. The detector can be either a Si-PIN photodiode for measurements in current mode or a Photo Multiplier Tube (PMT) for single photon counting. The Si-PIN photodiode (model Hamamatsu S-3584-08) is operative between 350 and 1100 nm whereas the PMT (Hamamatsu H-3164-10) is sensible between 300 and 650 nm. At present no monochromator is available but it is foreseen to achieve wavelength selection keeping a high luminosity by using bandpass filters. The installation of the filters is foreseen for the next year.

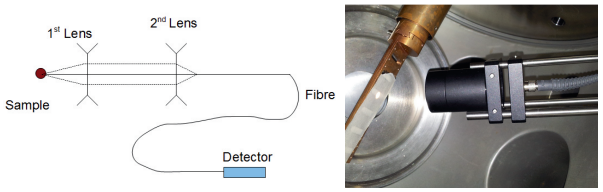

Figure 1: sketch and picture of the XEOL apparatus

The readout of both detectors is easily implemented in the standard XAS data collection system of GILDA. XAS-XEOL data have been collected with this apparatus on model compounds like ZnO; further spectra have been collected on different luminescent systems namely Mn-doped GaN (Ga-K edge), (Ce,Tb)-doped $Y_2Si_2O_7$ (Y K-edge), Er-doped SiO_2 nanoparticles. The apparatus is thus operative and available for user experiments.

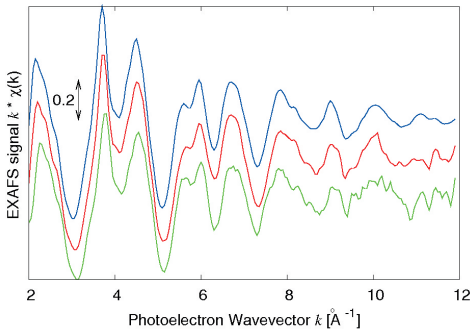

Figure 2: EXAFS spectra of ZnO in transmission mode (blue), XEOL with the PMT detector (red) and XEOL with the Si-PIN detector (green).

Cryostat for XAS experiments on frozen solutions

XAS experiments on biological samples are typically performed on frozen solutions in order to lower the thermal disorder and minimize the damage due to x-ray exposure. At this purpose, a liquid nitrogen bath cryostat has been recently commissioned and made available for users experiments on frozen liquids. Samples are loaded through the top of the cryostat and cooled by nitrogen exchange gas. With respect to the standard cryostat hosting sample holders attached to a cold finger, the device has the advantage of not needing vacuum around the sample. Solutions are measured in plastic cells covered with glued Kapton windows, smaller and thinner than those designed to be used in vacuum and disposable to prevent cross-contamination.

The 'hold time' is more than 12 hours at 80 K, allowing a full set of measurements to be collected without refilling and cooling down to 80 K is made in less than half an hour. The apparatus is compatible with both transmission and fluorescence detection modes. Two user experiments on diluted (~ 0.5 mM) protein samples have been successfully carried out.

2D X-ray fluorescence imaging

We have recently performed 2D x-ray fluorescence imaging experiments for the characterization of cm-sized zones of heterogeneous samples for which the extreme spatial resolution achieved with micro-beams is not needed. The x-ray spot size achievable on GILDA of 200 μm x 200 μm allows the collection of x-ray fluorescence maps on large areas (several mm^2).
Data collection can be carried out at different energies near the edge of an absorbing element in order to enhance the contribution from a particular valence state or site symmetry of the absorber. From the analysis of maps collected above the absorption edge and on selected features of the XANES such as the edge and pre-edge peak, it is possible to obtained qualitative information not only on the spatial distribution of the absorber inside the sample but also on its oxidation state and local symmetry.
This technique is applied both to scientific problems (in physics, materials science, environment, cultural heritage artefacts) and to purely industrial ones (reservoir rocks, composite materials, …) and it is important to note that in fluorescence detection, even the chemical state of trace elements with concentration in the ppm range can be studied.

The first experiments aimed to map the Cu content and oxidation state in fragments of Renaissance lustre pottery.

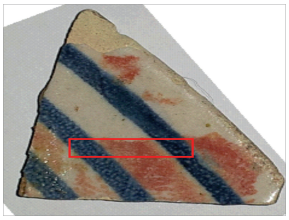

Figure1: optical image of a fragment of Umbrian Renaissance lustre pottery

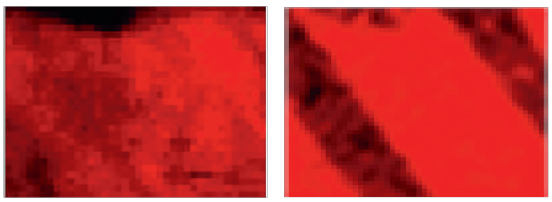

Figure 2: (left) Cu-Kα elemental map. (right): map collected at 8980 eV enhancing the contribution of Cu1+ ions. The sample is from the 'Museo Regionale della Ceramica di Deruta' and was provided by Prof. B.G. Brunetti of the University of Perugia.

Time resolved XAS studies

The participation of GILDA in the FEL-PIK project named EX-PRO-REL (EXcitation PROcesses and RELaxation in condensed matter and nanostructures) lead to the development of new capabilities for the beamline in the field of time-resolved studies.
In particular, our goal was the realization of pump and probe experiments exploiting the 16-bunch and 4-bunch filling modes of the ESRF storage ring. In these two timing modes, x-ray pulses of about 100 ps duration are available with a spacing of 176 and 704 ns respectively.
If combined with a pump signal at the same frequency and fixed time lag with the x-rays, a stroboscopic data collection can be realized without needing the use of fast detectors.
A first class of experiments was aimed to study structural deformation of (piezo/ferro)-electric materials like Lead Zirconium Titanate (PZT) under fast electrical excitation.
Small capacitors (dimensions 300 μm x 800 μm) consisting in 100nm-thick PZT were investigated with a sub-mm x-ray beam (200 μm x 200 μm) while applying intense electric field pulses (200 kV/mm, duration 200ns).
The pulse generator was especially realized for the project by the CNR-Istituto Officina dei Materiali electronics laboratory in Trieste.

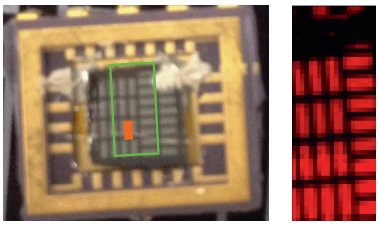

Figure 1: (left) picture of an array of PZT capacitors. The area mapped with x-ray fluorescence (green square) and the wired capacitor measured with x-rays (orange rectangle) are shown. Right: x-ray fluorescence map (Pt-L_α line)

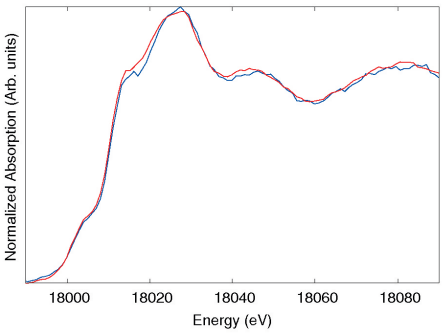

Figure 2: preliminary XANES spectra of PZT spectra with (blue) and without (red) excitation. These data show the feasibility of XAS measurements although we cannot draw any conclusion on the occurrence of structural distortions because the electrical contact to the capacitor was damaged during data collection.

Some problems encountered with samples are presently being addressed in order to complete this experiment, but the capability of data collection in stroboscopic mode has been fully demonstrated.
As an evolution of the technique, we plan to use it for light excitation with high power Light Emitting Diodes (LED) in the UV range, in 2014.

XAS at high energy using a Si(755)/Si(311) monochromator

GILDA beamline is designed to perform x-ray absorption spectroscopy (XAS) and powder diffraction in the 5-80 keV energy range using Si(111), Si(311) or Si(511) crystals on a sagittally focusing monochromator. Following the increasing demand for XAS measurements at different absorption edges spanning a wide energy interval within the same experiment, a straightforward system to extend the accessible energy range without intervention on the monochromator has been recently implemented.
In the past, a method based on the use of the 3rd harmonic of the Si(311) crystal was adopted, but the contamination from the fundamental and 4th harmonic revealed to pose problems.
Using the same principle we have adopted a new scheme based on a “split” first crystal, one half Si(311) and the other Si(755), each facing one half of the diamond-shaped Si(311) second crystal.
For a given incidence angle, the first (755) crystal selects three times the energy diffracted by Si(311) and can work with the second (bent) Si(311) crystal as the lattice spacing of its 3rd order reflection (933) is the same as 755. The white beam impinges on the Si(311) or Si(755) half of the first crystal depending on the primary slits horizontal offset and it is possible to access the 6-90 keV energy range [6-30 keV with the (311) and 30-90 keV with the (755)] without any intervention on the monochromator for crystal change that would heavily affect the beamline operation.
We have performed a number of tests to measure the flux and the signal to noise ratio achievable with this crystal mounting. The typical photon flux at the sample for standard ring current was in the 10^9 photons/s range allowing also measurments in fluorescence on diluted samples.
In Figure 1, we show the La K-edge absorption spectrum measured in fluorescence on a La doped (1 %mol) silicate glass and the corresponding XAFS signal.

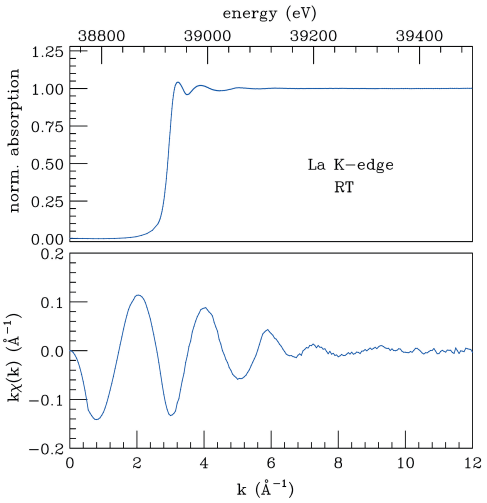

Fixed Energy X-ray Absorption Voltammetry (FEXRAV)

A. Minguzzi (a), O. Lugaresi (a), C. Locatelli (a), S. Rondinini (a), F. D'Acapito (b), E. Achilli (c) and P. Ghigna (c)

(a) Dipartimento di Chimica, Università degli Studi di Milano, Milan (Italy)
(b) CNR-IOM-OGG c/o ESRF, Grenoble (France)
(c) Dipartimento di Chimica, Università di Pavia, Pavia (Italy)

Fixed energy X-ray absorption voltammetry (FEXRAV) is a novel rapid XAS technique recently developed at GILDA, applied to electrochemical systems for the in situ study of electrode materials.
To describe the basic idea of FEXRAV we report, in Figure 1, the XAS spectra of IrO_2 (used as a standard for Ir^{4+}) and of $IrCl_3$ (used as a standard for Ir^{3+}) at the Ir-L_{III} edge.
It is evident that fixing the energy at the maximum of the absorption coefficient for IrO_2 (at 11221 eV, as indicated by the arrow) gives the maximum contrast between Ir^{3+} and Ir^{4+}.

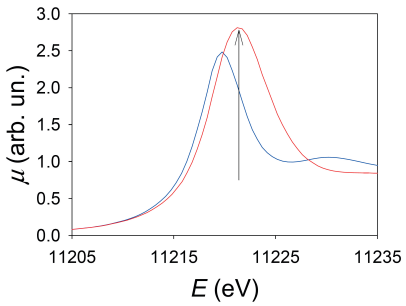

Figure 1: Normalized XANES spectra of IrO_2 (red) and $IrCl_3$ (blue). The arrow marks the energy chosen for the FEXRAV measurements (11221 eV).

With the X-Ray energy fixed at 11211 eV, the FEXRAV curve plotted in Fig. 2 evidences that, varying the potential applied at the electrode, the mean oxidation of Ir state crosses at least three different values.

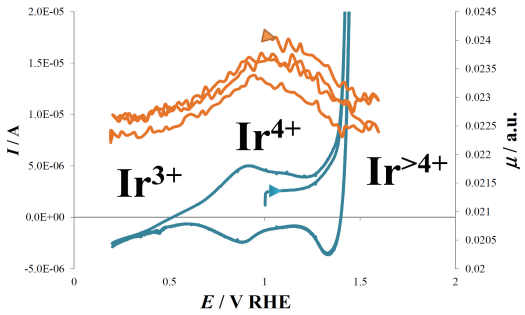

Figure 2: Conventional cyclic voltammetry (blue line) and the relevant FEXRAV curve (red lines) of iridium oxide recorded at 1 mV s-1.

For this experiment we designed a novel cell that allows to use thin electrodeposited iridium oxide films and to work in the fluorescence mode. FEXRAV allows to: (I) rapidly study any species that can be immobilized onto a conductive substrate, in terms of its oxidation state (or any other property that causes a change in the X-Ray absorption coefficient) in dependence on the applied potential, (II) screen samples for the application of more detailed local structural probes (XANES, EXAFS), (III) immediately define the potential windows at which each oxidation state is prevalent, (IV) extract important information on the reaction mechanisms, (V) extract kinetic constants or follow the reaction progression.
Also in this case, this is useful especially considering that the FEXRAV signal is not influenced by "parasitic" electrochemical phenomena.

Principal publication: A. Minguzzi *et al.*, Anal. Chem. **85** (2013), 7009-7013

EXAFS and XANES structural characterization of bimetallic AuPd vapor derived catalysts

A. Balerna (a), C. Evangelisti (b), E. Schiavi (c), G. Vitulli (d), L. Bertinetti (e), G. Martra (e), S. Mobilio (f,a)

(a) INFN-LNF, Frascati (Italy)
(b) CNR-ISTM Milano (Italy)
(c) Dep. of Chemistry, Pisa (Italy)
(d) Advanced Catalysis S.r.l., Pisa (Italy)
(e) Dep. of Chemistry IFM&NIS, Torino (Italy)
(f) Dep. of Physics, Univ. Roma Tre, Roma (Italy)

Using an innovative procedure known as metal vapor synthesis (MVS) to prepare bimetallic catalysts, starting from Au and Pd vapors, [AuPd] co-evaporated and [Au][Pd] separately evaporated bimetallic catalysts

were achieved.

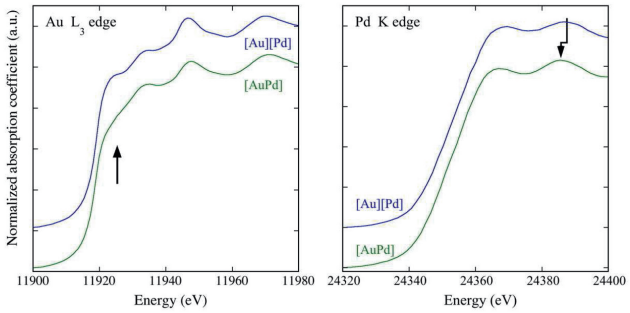

Figure 1 : XANES spectra at the Au L_3 and the Pd K edges.

After being tested, the catalytic activity and selectivity of the [AuPd] catalyst turned out to be higher than the [Au][Pd] ones. Using EXAFS spectroscopy it was shown that, in the [AuPd] samples, small bimetallic AuPd nanoparticles were present, having an Au rich core surrounded by an AuPd alloyed shell while in the [Au][Pd] sample there was the presence of monometallic Au and Pd nanoparticles showing some alloying only in the boundary regions.

The EXAFS results were also qualitatively confirmed by the XANES spectra. In Fig. 1, the peak indicated by the arrow at the Au L_3 edge is known as white line and its intensity is related to the presence of unoccupied 5d states.

In the nanoparticles, the reduced number of Au-Au bonds results in an increase in the 5d level occupancy and hence in a decrease in its intensity probably due to a charge transfer from Pd to Au. In the Pd XANES the shift observed in the [AuPd] sample is associated to the large amount of Au atoms around Pd.

Principal publication: A. Balerna *et al.*, Journal of Physics : Conference Series **430** (2013) 012052

X-ray diffraction and extended X-ray absorption fine structure study of epitaxial mixed ternary bixbyite $Pr_xY_{2-x}O_3$ films on Si(111)

G. Niu (a), M. H. Zoellner (a), P. Zaumseil (a), A. Pouliopoulos (b), F. d'Acapito (c), T. Schroeder (a) and F. Boscherini (b,c)

(a) IHP, Frankfurt (Germany)
(b) Department of Physics and Astronomy, University of Bologna, Bologna (Italy)
(c) CNR-IOM-OGG c/o ESRF, Grenoble (France)

Single crystalline bixbyite $Pr_xY_{2-x}O_3$ films (x=0–2) have been epitaxially grown on Si (111) with tailored electronic and crystallographic structure.

We present a detailed study of their local atomic environment by EXAFS at both Y K and Pr L_{III} edges, in combination with complementary XRD. The local structure exhibits systematic variations as a function of the film composition (Fig. 1, left). The cation coordination in the second and third coordination shells changes with composition and is equal to the average concentration, implying that the $Pr_xY_{2-x}O_3$ films have a local bixbyite structure with random atomic-scale ordering.

A clear deviation from the virtual crystal approximation for the cation-oxygen bond lengths is detected (Fig. 1, right). This demonstrates that the observed Vegard's law for the lattice variation is based microscopically on a more complex scheme related to local structural distortions which accommodate the different cation–oxygen bond lengths.

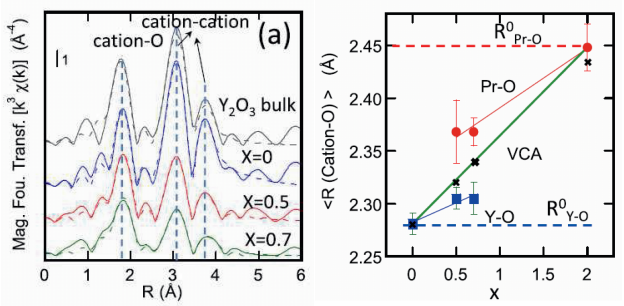

Figure 1: Fourier Transforms of Y edge EXAFS (left). Cation–oxygen bond lengths (right)

Principal publication: G. Niu *et al.*, Journal of Applied Physics **113** (2013) 043504

Influence of V doping on $LiFePO_4$ structure and electrochemical performance

A. Moretti (a), G. Giuli (a), F. Nobili (a), A. Trapananti (b), G. Aquilanti (c), R. Tossici (a) and R. Marassi (a)

(a) School of Science and Technology, University of Camerino, Camerino (Italy)
(b) CNR-IOM-OGG c/o ESRF, Grenoble (France)
(c) Sincrotrone Trieste, Trieste (Italy)

The interest in lithium-ion battery technology has grown exponentially in the last two decades. The main challenges in the development of lithium ion batteries for widespread commercial implementation are cost, safety, energy and power densities, charge/discharge rate and service life.
In this context, the olivine $LiFePO_4$ is considered the greenest, the safest and one of the cheapest materials able to replace the toxic and expensive cobalt oxides-based cathodes, although its use is hampered by the low intrinsic electronic and ionic conductivity. Nanosizing and carbon coating techniques are constantly developed to improve the electrochemical performances, at the expense of production costs and energy density.
Lattice engineering via transition metal doping seems to be a viable technique to obtain intrinsically electronic conductive phospho-olivine, although controversial results are reported in the literature. Among the different transition metals used as dopants, vanadium is one of the most intriguing because of the variety of oxidation states and possible structural roles in the olivine lattice.

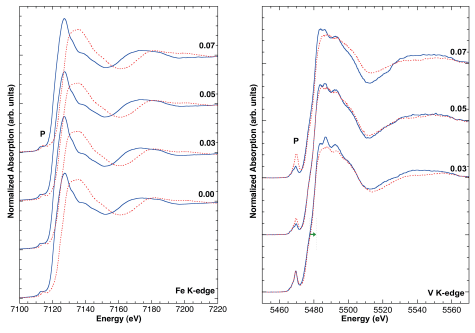

Figure 1: (left) Normalized Fe K-edge XANES spectra of reduced (blue solid lines) and oxidised electrodes (red dotted lines) with different V contents. (right). Normalized V K-edge XANES spectra of reduced (blue solid lines) and oxidised electrodes (red dotted lines) with different V contents (indicated in the label): unlike in the Fe K-edge XAS spectra, no energy shift is noticed upon cycling.

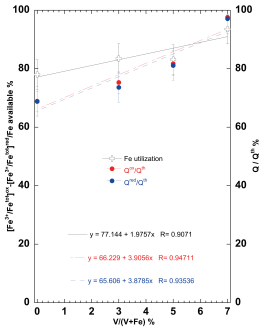

Figure 2: Fe utilization (left axis) calculated from Fe pre-edge peak analysis, as a function of the amount of vanadium inserted in the olivine lattice. The percentage of specific charge/discharge capacity (obtained from electrochemical tests) normalized to the theoretical values is also shown on the right axis.

With the aim of clarifying whether aliovalent doping of $LiFePO_4$ is possible or not, we synthesized a series of V-doped $LiFePO_4$ samples ($Li_{1-x}Fe_{1-x}V_xPO_4/C$ with $0<x<0.1$) and systematically studied the effect of the dopant on the crystal lattice parameters.
Structural data obtained from X-ray powder diffraction confirm that up to 7 at.% of V can be inserted into the olivine lattice without significant formation of secondary phases. Ex-situ XANES measurements on cycled electrodes at the V K-edge show the presence of V^{3+} in octahedral coordination and that V oxidation state remains unchanged upon cycling although the V-doped samples show improved electrochemical performance with respect to pure $LiFePO_4$, especially at high rates.
The XANES spectra at the Fe K-edge provide accurate Fe^{3+}/Fe^{2+} ratios for oxidised and reduced electrodes. The difference in the Fe^{3+} fraction between the oxidised and reduced electrodes has been interpreted as an indicator of the Fe utilization under a certain cycling rate and correlated with the V content and the delivered specific capacity.
These findings indicate that the substitution of V for Fe makes the iron redox process more efficient leading to an improvement of the electrochemical performance of the $LiFePO_4$ cathode material. This enhanced electrochemical performance may be linked to the creation of Li vacancies and local structural distortion around V, and to the extension of the solid solution behaviour.

Principal publication: A. Moretti *et al.*, J. Electrochem. Soc. **160** (2013), A940–A949

Variability of the health effects of crystalline silica: Fe speciation in industrial quartz reagents and suspended dusts – insights from XAS spectroscopy

F. Di Benedetto (a), F. D'Acapito (b), F. Capacci (c), G. Fornaciai (d), M. Innocenti (d,e), G. Montegrossi (f), W. Oberhauser (e), L. A. Pardi (g) and M. Romanelli (a)

(a) Dip. Scienze della Terra, Univ. Firenze, Firenze (Italy)
(b) CNR-IOM-OGG, c/o ESRF, Grenoble (France)
(c) ASF, (Italy)
(d) Dip. Chimica, Univ. Firenze, Firenze (Italy)
(e) CNR-ICCOM Sesto Fiorentino, (Italy)
(f) CNR-IGG Firenze, Firenze (Italy)
(g) CNR-IPCF Pisa, Pisa (Italy)

The speciation of Fe in bulk and suspended respirable quartz dusts coming from ceramic and Iron casting industrial processes is investigated through XAS, with the aim of contributing to unravel the variability of crystalline silica toxicity.
Fe speciation reveals common features at the beginning of the different production processes, whereas significant differences are observed on both respirable dusts and bulk dusts exiting from the production process.
Namely, a common pollution of the raw quartz dusts by elemental Fe was evidenced and attributed to residuals of the industrial production of quartz materials (Fig. 1).
Moreover, the respirable samples indicate that reactivity occurs after the suspension of the powders in air. The gravitational selection during the particle suspension always allows to clearly discriminate suspended and bulk dusts.
On the basis of the obtained results, an apparent spectroscopic discrimination is provided between the raw materials used in the considered industrial processes, and those effectively breathed from workers. In particular, an amorphous FeIII oxide, with unsaturated coordination sphere (Fig. 2), can be related to silica reactivity (and health consequences).

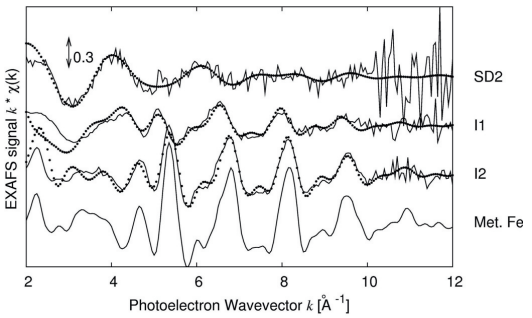

Figure 1: XAS spectra in the EXAFS region of samples I1, I2 (bulk dusts) and SD2 (respirable dusts), compared with reference metallic Fe, in k space.

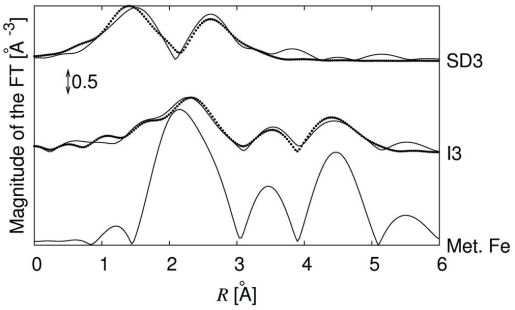

Figure 2: Magnitude of the Fourier transform of the EXAFS spectra for I3 (bulk dusts) and SD3 (respirable dusts) compared to reference metallic Fe, in R space.

Principal publication: F. Di Benedetto *et al.*, Phys. Chem. Minerals (2014), in press

Speciation of arsenic in Greek travertines: co-precipitation of arsenate with calcite

L. H. E. Winkel (a,b), B. Casentini (c,a,e), F. Bardelli (d), A. Voegelin (a), N. P. Nikolaidis (e), L. Charlet (d)

(a) EAWAG, Zurich (Switzerland)
(b) ETH, Zurich (Switzerland)
(c) Water Research Institute-CNR, Rome (Italy)
(d) ISTerre, Grenoble (France)
(e) Technical University of Crete, Chania (Greece)

Geogenic arsenic contamination of groundwater is a serious environmental health threat in many countries. Many natural minerals or engineered materials can uptake considerable amounts of arsenic. In particular, calcite ($CaCO_3$) can play an important role in limiting the mobility of As because of its ubiquity in the Earth's crust and its stability in a variety of geologic environments. The western part of the Chalkidiki

peninsula in Northern Greece is such an area that is affected by high As concentrations in the groundwater, with reported As levels reaching 3760 µg/L.

Our XAS studies showed that in all of the studied samples arsenic is present in the pentavalent oxidation state and in a local environment that is typical of arsenate species. Micro-XRF analyses showed that arsenic is closely associated with the calcite matrix and that it generally does not correlate well with iron. These results were confirmed by XAS analyses, which indicated that arsenic is probably incorporated in the calcite lattice and had thus coprecipitated with calcite (Figures 1 and 2).

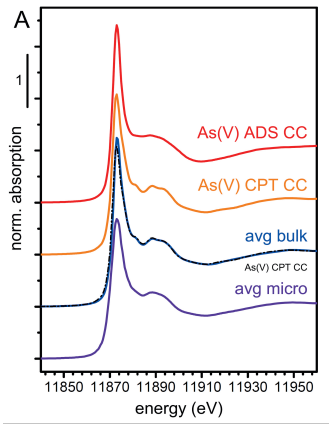

Figure 1: As K-edge XANES spectra of reference samples for As(V) adsorbed (ADS) on calcite (CC) (solid red line) and coprecipitated (CPT) with calcite (CC) (solid orange line). Avg bulk: average of all bulk spectra collected at GILDA beamline. Avg micro: average of all µXANES spectra measured at SulX beamline.

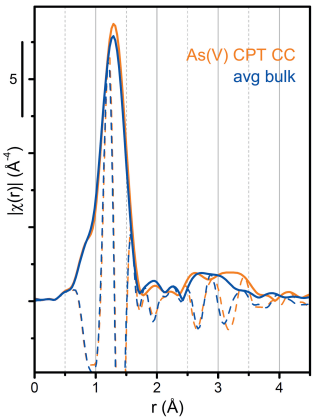

Figure 2: Comparison of the Fourier-transformed reference spectrum of As(V) coprecipitated with calcite (orange) and of the average spectrum from all bulk samples (blue). Solid lines: magnitude. Dotted lines: imaginary part.

On the other hand, iron was found to be mainly present in the form of clay minerals. Results suggest that iron bearing phases such as iron-(hydr)oxides were not sufficiently abundant to act as major scavenger for arsenic in the Chalkidiki travertines. We estimated that calcite in these travertines could sequester at least 25% of aqueous arsenic (As[V]), immobilizing a substantial part of arsenic present in the geothermal groundwaters.

Principal publication: L.H.E. Winkel *et al.*, Geochim. Cosmochim. Acta **106** (2013), 99

Natron-based yellow, blue-green and colourless Roman soda-lime silica glasses

E. Gliozzo (a), A. Santagostino Barbone (b) and F. d'Acapito (c)

(a) Department of Physical, Earth and Environmental Sciences, University of Siena (Italy)
(b) Opificio delle pietre dure, Firenze (Italy)
(c) CNR-IOM-OGG c/o ESRF, Grenoble (France)

An important issue in the reconstruction of Roman glass technology is to to tell whether the furnace atmosphere or the quantitative predominance of a chromophore over the other plays the major role in glass colouring.
XAS measurements are able to provide an insight on these colouring agents, therefore investigations at the Fe and Mn-K edges were performed on: 1) dark aqua blue glasses, with Fe_2O_3 > MnO < 0.22 wt%; 2) light aqua blue glasses, with Fe_2O_3 < MnO = 0.42-0.65 wt%; 3) light yellow/green and colourless glasses with Fe_2O_3 < MnO > 1 wt%); 4) Sb-rich (>1500 ppm) colourless glasses, with Fe_2O_3 >> MnO < 1 wt%; 5) amber glasses, with Fe_2O_3 and MnO < 0.5 wt%.
The results showed a very low Fe^{3+}/Fe^{tot} ratio (48% and 50% respectively) in the first group, thus indicating the predominance of Fe^{2+} ions for colour development.
In the second group, the Fe^{3+}/Fe^{tot} ratio increased to 70%, with Mn being in the (II) state of Mn. In this instance, low amounts of Mn partially oxidised Fe^{2+} but warranted the aqua blue colour to the glass. Also, with respect to the previous one, their lighter hue was explained by the increased Fe^{3+}/Fe^{tot} ratio.
The third group showed two cases: 1) with Fe^{3+}/Fe^{tot} ratio > 75% and Mn in the (II) state, the reduction of the latter to Mn^{2+} was effective in oxidizing almost all Fe^{2+} to Fe^{3+}, and a light colouration was still ensured to the glass; 2) with Fe^{3+}/Fe^{tot} ratio decreased to 64% the glass appeared colourless.

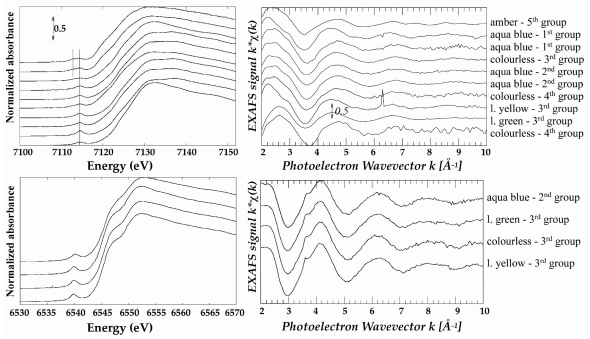

Figure 1: X-ray Absorption Spectroscopy at the Fe- and Mn-K edges. A) XANES full spectra at the Fe-K edge. The long line at the right indicates the edge position of Fe3+, while the short line at the left the one of Fe2+; B) EXAFS data; C) XANES full spectra at the Mn-K edge; D) EXAFS data.

In the fourth group, the Fe^{3+}/Fe^{tot} ratio was over 80%, hence able to confer a pale yellow hue to the glass easily modifiable into colourless using just rare Ca antimonates. The main effect of Sb may have been as oxidizing agent. Surprisingly, both Fe^{3+} (39% Fe^{3+}/Fe^{tot}) and Fe^{2+} were identified in the 5th group, where the ferric iron sulphide complex (Fe^{3+}–S^{2-}) developed the amber colour.
The dark hue was then related to the considerable amount of ferrous iron in the glass.

Principal publication: E. Gliozzo *et al.*, Archaeometry **55** (2013), 609-639

Chromophores in archaeological glass: a XANES study

R. Arletti (a), S. Quartieri (b) and I. C. Freestone (c)

(a) Dipartimento di Scienze della Terra, Università di Torino (Italy)
(b) Dipartimento di Fisica e Scienze della Terra, Università di Messina (Italy)
(c) Institute of Archaeology, London (United Kingdom)

The evaluation of the oxidation state of coloring elements in ancient glass offers important information not only about the origin of color, but also on the production technology employed in ancient times.
In fact, oxygen fugacity is one of the parameters which had to be carefully controlled by the ancient glass workers, as this variable was extremely important in determining the final glass color.
Fe and Mn K-edge XANES have been applied to study a series of selected colored glass fragments – mainly from excavated primary and secondary production

centers and dated to the first millennium AD – containing these two chromophores in a wide compositional range (Figure 1).

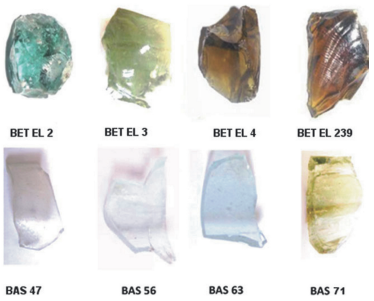

Figure 1: Pictures of selected glass samples

In most of the studied samples iron is rather oxidized (Figure 2), while Mn is always present in its reduced forms (predominantly 2+ and subordinately 3+).

The most oxidized samples are HIMT (high iron manganese titanium) glasses, while the less oxidized ones belong to a primary natron glass series from the early Islamic tank furnaces at Bet Eliezer (Israel), and to a series coming from a Roman glass workshop excavated in Basinghall Street, London.

Overall, these results suggest that primary natron glass was typically produced under moderately reducing conditions, where Fe^{3+} represents 50–70%of the total iron. More oxidized glasses appear to have been produced by adding an oxidizing agent, such as manganese or antimony oxide to the glass. The XANES analyses of two glasses which had been deliberately decolorized using Sb- and Mn-based decolorizers demonstrate that Sb is more effective than Mn as oxidant.

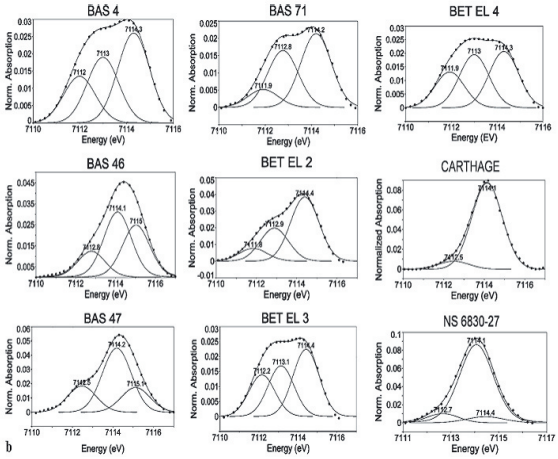

Figure 1: Normalised Fe K-pre-edge spectra and the best-fit model calculated for the glass samples

Principal publication: R. Arletti *et al.*, Appl Phys A, **111** (2013) 99

Ion binding sites in lipid membranes

M. Bergamino (a,d), A. Relini (a), P. Rispoli (a,e), L. Giachini (b), F. d'Acapito (c) and R. Rolandi (a)

(a) Department of Physics, University of Genoa (Italy)
(b) Department of Physics, University of Bologna (Italy)
(c) CNR-IOM-OGG c/o ESRF, Grenoble (France)
(d) Department of Neuroscience, Rehabilitation, Ophthalmology, Genetics, Maternal and Child Health, University of Genoa (Italy)
(e) Present address: Department of Physics, University of Rome, "La Sapienza", 00185 Rome (Italy)

Metal cation binding strongly affects the structure and stability of cell membranes as well as those of artificial lipid membranes.
The ability of cations to determine the molecular order in lipid membranes is best studied in Langmuir-Blodgett (LB) films, which are among the early and best-studied examples of artificially assembled ordered molecular systems.
In the work highlighted here, we have demonstrated, by ReflEXAFS measurements, that the different structures induced in fatty acid LB films by cadmium and lead ions correspond to different coordination structures.
In particular, in cadmium stearate (CdSt2) films, the coordination of Cd was found to be quite similar to that of cadmium in acetate aqueous solutions. Six oxygen atoms form the inner shell and two carbon atoms form the outer shell, consistent with unidentate coordination. In lead stearate (PbSt2) films, an O-shell containing oxygen atoms from a carboxyl group and hydration water molecules, and a C-shell formed by the carbon atom of a carboxyl group best describe Pb coordination. This coordination is consistent with a bidentate coordination.

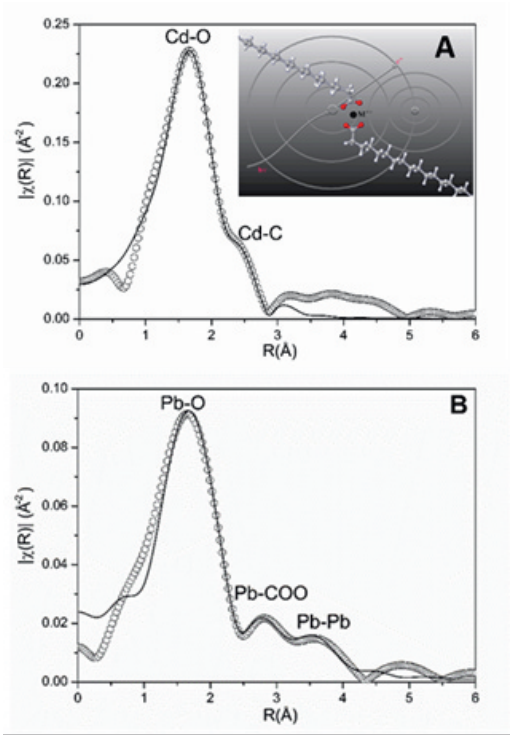

Figure 1: Fourier transforms of EXAFS spectra of LB films of A) CdSt2 and B) PbSt2; correspondences between peaks and paths are indicated. The inset shows a sketch of the mutual position of the metal ion and stearic acid molecules.

Furthermore, the Pb ion also coordinates other three Pb ions justifying the long-range order of the monolayers of fatty acids containing Pb ions. We have also studied the Cd and Pb coordination in phospholipid LB films and we observed that Pb-Pb coordination is absent in these films.

Principal publication: M. Bergamino *et al.*, Eur. Phys. J. E Soft Matter, **36** (2013) 102

List of publications

1) Arletti R., Quartieri S., Freestone I.C., *A XANES study of chromophores in archaeological glass,* Applied Physics A **111**, 99 (2013)

2) Aurelio G., Bardelli F., Junqueira Prado R., Sánchez R. D., Saleta M. E., Garbarino G., *On the location of host Ca atoms responsible for ferrimagnetism in the layered cobaltites* $YBaCo_2O_{5.5}$, Chemistry of Materials **25**, 3307 (2013)

3) Balerna A., Evangelisti C., Schiavi E., Vitulli G., Bertinetti L., Martra G., Mobilio S., *EXAFS and XANES structural characterization of bimetallic AuPd vapor derived catalysts*, Journal of Physics: Conference Series **430**, 012052 (2013)

4) Bergamino M., Relini A., Rispoli P., Giachini L., d'Acapito F., Rolandi R., *An EXAFS study of the binding of Cd and Pb ions to lipid films*, The European Physical Journal E **36**, 102 (2013)

5) Biagioni C., Bonaccorsi E., Merlino S., Bersani D., *New data on the thermal behavior of 14 Å tobermorite*, Cement and Concrete Research **49**, 48 (2013).

6) Bordiga S., Groppo E., Agostini G., van Bokhoven J.A., Lamberti C., *Reactivity of surface species in heterogeneous catalysts probed by in situ X-ray absorption techniques*, Chemical Reviews **113**, 1736 (2013)

7) Boscherini F., *Chapter 7 - X-ray absorption fine structure in the study of semiconductor heterostructures and nanostructures*, in Characterization of Semiconductor Heterostructures and Nanostructures II, pp. 259-310, Eds. G. Agostini and C. Lamberti, Elsevier, 2013.

8) Centomo P., Meneghini C., Zecca M., *Versatile plug flow catalytic cell for in situ transmission/fluorescence x-ray absorption fine structure measurements*, Review of Scientific Instruments **84**, 054102 (2013)

9) d'Acapito F., Pochet P., Somma F., Aloe P., Montereali R.M., Vincenti M.A., Polosan S., *Lead incorporation mechanism in LiF crystals*, Applied Physics Letters **102** 081107 (2013)

10) Di Benedetto F., d'Acapito F., Bencista I., Luca A., Fornaciai G., Frizzera S., Innocenti M., Montegrossi G., Pardi L.A., Romanelli M., *Preliminary XAS investigations on some phases of the Cu-Sn-S system*, Physica Status Solidi (c) **10**, 1055 (2013)

11) Gigli L., Arletti R., Quartieri S., Di Renzo F., Vezzalini G., *The high thermal stability of the synthetic zeolite K–L: Dehydration mechanism by in-situ SR-XRPD experiments*, Microporous and Mesoporous Materials **177**, 8 (2013).

12) Gliozzo E., Santagostino Barbone A., d'Acapito F., *Waste glass, vessels and window-panes from Thamusida (Morocco): Grouping Natron-based Blue-green and Colourless Roman Glasses*, Archaeometry **55**, 609 (2013)

13) Kang M., Ma B., Bardelli F., Chen F., Liu C., Zheng Z., Wu S., Charlet L., *Interaction of aqueous Se(IV)/Se(VI) with FeSe/FeSe2: Implication to Se redox process*, Journal of Hazardous Materials **248-249**, 20 (2013)

14) Leardini L., Martucci A., Cruciani G., The unusual thermal behaviour of boron-ZSM-5 probed by “in situ” time-resolved synchrotron powder diffraction, Microporous and Mesoporous Materials **173**, 6 (2013)

15) Luches P., Pagliuca F., Valeri S., Boscherini F., *Structure of ultrathin CeO2 films on Pt(111) by polarization-dependent* X-ray Absorption Fine Structure, Journal of Physical Chemistry C **117**, 1030-1036 (2013)

16) Medas D, Lattanzi P, Podda F, Meneghini C, Trapananti A, Sprocati A, Casu MA, Musu E, De Giudici G (2013), *The amorphous Zn biomineralization at Naracauli stream, Sardinia: electron microscopy and X-ray absorption spectroscopy*, Environ. Sci. Pollut. R., online, doi:10.1007/s11356-013-1886-4

17) Minguzzi A., Lugaresi O., Locatelli C., Rondinini S., d'Acapito F., Achilli E., Ghigna P., *Fixed energy X-ray absorption voltammetry*, Analytical Chemistry **85**, 7009 (2013)

18) Mohiddon M.A., Naidu K.L., Dalba G., Rocca F., Krishna M.G., *Crystalline silicon growth in nickel/a-silicon bilayer*, AIP Conference Proceedings **1512**, 686 (2013)

19) Monteiro G., Santos L.F., Almeida R.M., d'Acapito F., *Local structure around Er3+ in* GeO_2-TeO_2-Nb_2O_5-K_2O *glasses and glass-ceramics*, Journal of Non-Crystalline Solids **377**, 129-136 (2013)

20) Moretti A., Giuli G., Nobili F., Trapananti A., Aquilanti G., Tossici R., Marassi R., *Structural and electrochemical characterization of vanadium-doped LiFePO4 cathodes for lithium-ion* batteries, Journal of the Electrochemical Society **160**, A940 (2013)

21) Naidu K.L., Mohiddon M.A., Krishna M.G., Dalba G., Rocca F., *Metal induced crystallization of amorphous silicon thin films studied by x-ray absorption fine structure spectroscopy*, Journal of Physics: Conference Series **430** 012035 (2013)

22) Niu G., Zoellner M.H., Zaumseil P., Pouliopoulos A., d'Acapito F., Schroeder T., Boscherini F., *X-ray diffraction and extended X-ray absorption fine structure study of epitaxial mixed ternary bixbyite* $Pr_xY_{2-x}O_3$ *(x=0–2) films on*

List of publications

Si (111), Journal of Applied Physics **113**, 043504-1 (2013)
23) Parsons C.T., Couture R.M., Omoregie E.O., Bardelli F., Grenèche J.M., Román-Ross G., Charlet L., *The impact of oscillating redox conditions: Arsenic immobilisation in contaminated calcareous plain soils*, Environmental Pollution **178**, 254 (2013)
24) Pin S., Suardelli M., d'Acapito F., Spinolo G., Zema M., Tarantino S.C., Barba L., Ghigna P., *Role of Interfacial Energy and Crystallographic Orientation on the Mechanism of the ZnO + Al_2O_3 → $ZnAl_2O_4$ Solid-State Reaction: II. Reactivity of Films Deposited onto the Sapphire (001) Face*, Journal of Physical Chemistry C **117**, 6113 (2013)
25) Pin S., Suardelli M., d'Acapito F., Spinolo G., Zema M., Tarantino S.C., Ghigna P., *Role of Interfacial Energy and Crystallographic Orientation on the Mechanism of the ZnO + Al_2O_3 → $ZnAl_2O_4$ Solid-State Reaction: I. Reactivity of Films Deposited onto the Sapphire (110) and (012) Faces*, Journal of Physical Chemistry C **117**, 6105 (2013)
26) Pompeo N., Torokhtii K., Meneghini C., Mobilio S., Loria R., Cirillo C., Ilyina E.A., Attanasio C., Sarti S., Silva E., *Superconducting and structural properties of Nb/PdNi/Nb trilayers*, Journal of Superconductivity and Novel Magnetism **26**, 1939 (2013)
27) Ramamoorthy R.K., Bhatnagar A.K., Vachhani P.S., Dalba G., Grisenti R., Mattarelli M., Montagna M., Armellini C., Rocca F., *Investigation of Er3+ coordination in zinc-lead tellurite bulk glasses and silica-hafnia glass* ceramics waveguides, Journal of Physics: Conference Series **430**, 012089 (2013)
28) Sipr O., Vackar J., Vachhani P.S., Ramamoorthy R.K., Dalba G., Bhatnagar A.K., Rocca F., *Local structure and magnetism of Cu-doped ZnO via Cu K-edge XAS and XMCD: Theory and experiment*, Journal of Physics: Conference Series **430** 012128-1 (2013)
29) Taglieri G., Mondelli C., Daniele V., Pusceddu E., Trapananti A., *Synthesis and X-ray diffraction analyses of calcium hydroxide nanoparticles in aqueous suspension*, Advances in Materials Physics and Chemistry **3**, 108 (2013)
30) Varrica D., Bardelli F., Dongarrà G., Tamburo E., *Speciation of Sb in airborne particulate matter, vehicle brake linings, and brake pad wear residues*, Atmospheric Environment **64**, 18 (2013)
31) Winkel L.H.E., Casentini B., Bardelli F., Voegelin A., Nikolaidis N.P., Charlet L., *Speciation of arsenic in Greek travertines: Co-precipitation of arsenate with calcite*, Geochimica et Cosmochimica Acta **106**, 99 (2013)

Applications for beamtime

GILDA beamline has two third of its operational beamtime available for Italian users experiments (CRG quota). Two proposal review rounds are held each year. Deadlines for applications to make **use of the CRG beamtime** are normally, **1st May and 1st November**. A reminder is e-mailed to our users shortly before the deadline. Applications for beamtime must be submitted electronically on the ESRF User Portal. Follow the instructions carefully and remember to choose "CRG Proposal" and "GILDA-Hutch XAS" at the appropriate stage in the process. A detailed description of the submission process is also available on the GILDA webpage **http://www.esrf.eu/UsersAndScience/Experiments/CRG/BM08**.

For any advice and support feel free to contact the GILDA staff: Francesco d'Acapito (dacapito@esrf.fr), Angela Trapananti (trapananti@esrf.fr) and Simona Torrengo (torrengo@esrf.fr).

GILDA beamline is also available for one third of its operational beamtime to the ESRF's user community. Applications for the **ESRF beamtime** quota should be made within the ESRF's proposal dedlines, **1st March and 1st September.**

GILDA beamline c/o European Synchrotron Radiation Facility
6 rue Jules Horowitz , BP 220
F-38043 Grenoble Cedex 9 (France)

Tel: +33 (0)476882085

http://www.esrf.eu/UsersAndScience/Experiments/CRG/BM08
e-mail: dacapito@esrf.fr

Acknowledgements

The GILDA staff is indebted to a long list of collaborators for contributing to the experiments and achievements of the present year. In particular we wish to thank E. Dettona and S. Ohlsson (ESRF), V. Tullio (INFN-LNF), A. Martin (CNR-IOM) for their technical help.

We gratefully acknowledge R. Arletti, A. Balerna, F. Bardelli, F. Boscherini, L. Cartechini, F. di Benedetto, E. Gliozzo, G. Giuli, A. Minguzzi and R. Rolandi for their contributions to this first issue of the GILDA annual report.